ISSN 1392-1207. MECHANIKA. Vol. 31, No. 2, 2025: 87–95

Effect of Nanoscale Amorphization on Edge Dislocation Emission from a Bifurcated Crack Tip in Deformed Nanocrystalline Solids

Xiaoya SONG*, Min YU, Xianghua PENG*****
**Hunan Province Key Laboratory of Engineering Rheology, Central South University of Forestry and Technology, Changsha 410004, PR China, E-mail: 20211100398@csuft.com*
***Hunan Province Key Laboratory of Engineering Rheology, Central South University of Forestry and Technology, Changsha 410004, PR China, E-mail: T20061781@csuft.com (Corresponding Author)*
****College of Information Science and Engineering, Hunan Women's University, Changsha 410004, PR China, E-mail: pengxianghua@hnwu.edu.cn (Corresponding Author)*
https://doi.org/10.5755/j02.mech.40198

1. Introduction

Due to the small grain size of nanocrystalline materials, the internal interfaces composed of grain boundaries, phase boundaries, or domain boundaries are very high. Grain boundaries can account for 50% or more of the entire material, making its performance different from that of crystals or amorphous materials with the same composition. The high grain boundary density of nanocrystalline materials can increase their strength by an order of magnitude, and due to their unique composition and structure, their performance is significantly improved and enhanced compared to traditional materials, especially with special properties such as super-hard and super-modulus effects [1-22]. However, the low tensile elongation and high brittleness exhibited by nanocrystalline materials limit their application. Therefore, when it was discovered that certain specific nanocrystalline materials can exhibit superplasticity and super toughness at high temperatures, or exhibit good tensile ductility at room temperature, this greatly aroused the interest of researchers. At present, most studies indicate that these characteristics are attributed to special deformation mechanisms in nanocrystalline materials, such as special rotational deformation [23], grain boundary slip and migration [24], nano amorphization [25], Coble creep [17], etc.

Nanoscale amorphization, which is the transition from a crystalline to an amorphous state at the nanoscale, is a unique deformation mechanism commonly observed in nanocrystalline materials. Many experiments and theories currently suggest that nanoscale amorphization significantly influences the toughness of materials. It also plays a crucial role in the plastic deformation process of nanocrystalline materials. Ovid'ko and Sheinerman [26-29] propose that during the splitting transformation process, grain boundary dislocations move, resulting in local plastic deformation that relaxes the stress caused by wedge disclination dipoles. Grain boundary dislocations are distinct from lattice dislocations, and their movement creates a disordered region known as the amorphous region, composed of these dislocations. They also observed that nanocrystalline materials can undergo amorphization at grain boundaries and their triple junctions even without an external load, acting as a mechanism to relax elastic energy through grain boundary dislocations (rotational defects). Furthermore, it has been noted that nanoscale amorphization occurs near the crack tip and can impede crack propagation. However, the actual cracks in nanocrystalline solids are relatively complex, and their configurations are diverse. To some extent, internal cracks, which consist of the main crack and its branches, can more accurately depict the real crack [30].

The article adopts a theoretical model that characterizes nanoscale amorphous regions within nanocrystalline materials using n pairs dislocation dipoles [25]. Subsequently, a mechanical model was established to investigate the effect of nanoscale amorphous regions near the tip of bifurcated cracks on crack passivation. By employing the method of complex potential functions in elasticity, the resultant force acting on dislocations is analyzed, and an analytical expression for the critical SIF (Stress Intensity Factor) corresponding to dislocation emission at the tip of the bifurcated crack is derived. Additionally, the study examines the variation of typical parameters, such as nanoscale amorphization, dislocation emission angle, and the relative length between the main and branched cracks, on dislocation emission at the tip of the bifurcated crack. The influence of these parameters on the toughness of nanocrystalline materials is also explored.

2. Establishment of Mechanical Models

As depicted in Fig. 1, an infinite nanocrystalline solid is subjected to in-plane shear loading (Mode II) and tensile loading (Mode I) at infinity. The solid material is segmented into nanocrystals delineated by grain boundaries (GBs), which encompass a bifurcated crack within, as illustrated in Fig. 1, a. The magnified view and mapped ζ-plane of nanoscale amorphization near the bifurcated crack tip are depicted in Fig. 1, b and Fig. 1, c, respectively.

Assuming the nanocrystalline solid is uniformly isotropic, the lengths of the main crack and the branched crack are expressed as a and b, respectively, and the internal angle between them is $(1-m)\pi$. Without loss of generality, we assume that the length of the branched crack does not exceed that of the main crack, namely $b \le a$. It is known that the shear modulus is μ and the Poisson's ratio is ν. The material is subjected to far-field mode I and mode II loads. The defect structure is identical in the direction perpendicular to the plane of the main crack and the branched crack. Based on this assumption, we can establish a two-dimensional mechanical model to analyze the primary aspects of the problem.

Two coordinate systems are introduced: the Cartesian coordinate system (x', y') and the Polar coordinate system, with the origin at the right end of the branched crack,

as shown in Fig. 1, b.

Referring to Feng's work [25], for the rectangular amorphous region near the bifurcated crack tip, it is assumed that the lattice dislocations are continuously distributed at a constant density. Therefore, the amorphization within the rectangular region can be equivalent to *n* pairs of wedge disclination dipoles uniformly distributed on the lateral boundaries *AD* and *BC*, as shown in Fig. 1, c.

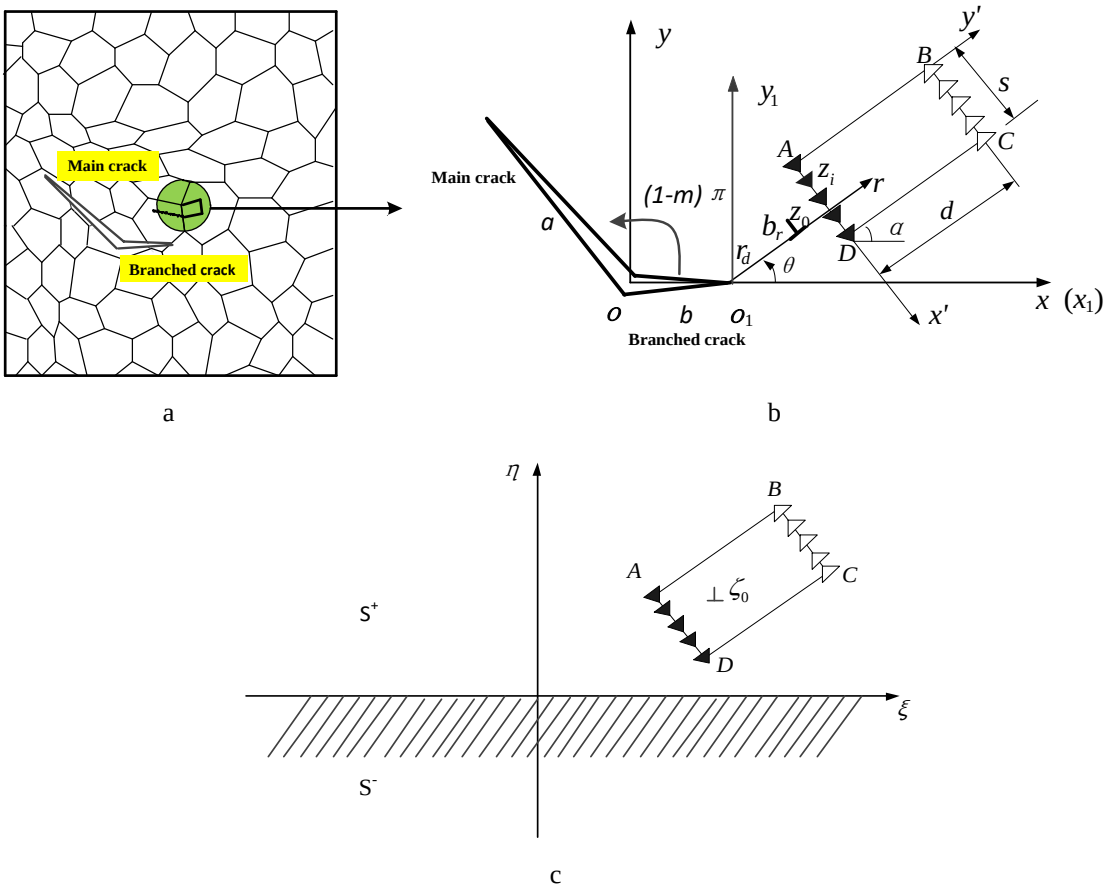

Fig. 1 A two-dimensional mechanical model illustrating the effect of nanoscale amorphization on dislocation emission from a bifurcated crack tip in nanocrystalline materials: a – general view, b – enlarged view, c – the mapped ζ-plane

3. Calculation of Forces Acting on the First Edited Edge Dislocation

It is widely recognized that if the stress level at the vicinity of a crack's end becomes sufficiently elevated, the crack will initiate the release of lattice dislocations from its tip, which in turn facilitates the plastic deformation of the surrounding material. The mechanical behavior of the bifurcation crack needs to be analyzed. The emission of the first edge dislocation from this crack is a critical event, as it initiates the process of crack propagation. To understand this phenomenon, it is essential to consider the interplay between the various forces acting on the dislocation.

The force generated by nanoscale amorphization plays a significant role, as it drives the dislocation to move along the crack surface. Additionally, the image force of the dislocation itself also contributes to its motion. This force arises due to the interaction between the dislocation and its image in the adjacent crystal lattice. Finally, the force generated by external loads, such as tensile or compressive stresses, can also influence the emission and propagation of the dislocation. By carefully analyzing these forces, we can develop a comprehensive mechanical model that describes the behavior of the bifurcated crack and the associated dislocation emission process. So, when the first edge dislocation is emitted from the bifurcation crack, the total emission force acting on it comprises three components: the force generated by nanoscale amorphization f_{Ae}, the image force of the dislocation itself f_{Ie} and the force generated by external loads f_{Ie}.

Firstly, when we consider the force generated by nanoscale amorphization, it is essential to understand the fundamental principles behind this phenomenon. Amorphization at the nanoscale refers to the process where materials undergo a transition from a crystalline state to an amorphous state, which is characterized by a lack of long-range order in the atomic structure. This transformation can be induced by various means, such as irradiation, mechanical deformation, or chemical reactions, and it often results in significant changes in the physical and mechanical properties of the material. In the context of our discussion, we are particularly interested in the force that arises due to this amorphization process. Assuming that the first edge dislocation of Burgers vector $b_r e^{i\theta_0}$ is located at point $z_0 = b_r + r_0 e^{i\theta_0}$, we can delve into the specifics of how this dislocation contributes to the force generated by nanoscale amorphization. The point at which this dislocation is located is significant because it marks the site where the structural irregularity begins, and it is from this point that the force exerted by the amorphization process emanates. The force f_{Ae} generated by nanoscale amorphization can be expressed mathematically

as [25, 31]:

$$f_{Ae} = b_r \sigma_{r\theta}^N = \\ = b_r \left[\left(\sigma_{yy}^N - \sigma_{xx}^N \right) \sin\theta \cos\theta + \sigma_{xy}^N \cos 2\theta \right], \quad (1)$$

where: σ_{xx}^N, σ_{yy}^N and σ_{xy}^N are the stress field components formed by nanoscale amorphization near a bifurcation crack in deformed nanocrystalline solids.

Nanoscale amorphization is represented by *n* pairs of wedge disclination dipoles, so the stress fields σ_{xx}^D, σ_{yy}^D and σ_{xy}^D generated by a wedge disclination with strength ω at point $z_i = x_i + iy_i$ in nanocrystalline solids with a bifurcated crack should be derived.

Introduce the following conformal transformation function to map the infinite region outside the internal crack in the *z*-plane to the infinite region inside the ζ-plane [31]:

$$z = \omega\ \zeta\ = 2R\ 1 + \cos\alpha\ e^{i\pi\ 1-m} \times \frac{\left(\zeta - tan\frac{\alpha}{2}\right)^{1+m} \left(\zeta + tan\frac{\alpha}{2}\right)^{1-m}}{\zeta^2 + 1} \quad 0 \le m < 1\ , \quad (2)$$

where:

$$\left.\begin{aligned} a &= 4R\left[cos\left(\frac{\alpha+\beta}{2}\right)\right]^{1-m}\left[cos\left(\frac{\alpha-\beta}{2}\right)\right]^{1+m} \\ b &= 4R\left[cos\left(\frac{\alpha+\beta}{2}\right)\right]^{1+m}\left[cos\left(\frac{\alpha-\beta}{2}\right)\right]^{1-m} \end{aligned}\right\}, \quad (3)$$

and $\zeta = \eta + i\xi$, $sin\beta = m\ sin\alpha$, *R* is a real constant. The parameters α and β can be determined by assigning values to *m* and the length ratios *b*/*a*, and *b*/*a* ≤ 1.

Taking the derivative yields:

$$z' = \omega'(\zeta) = \frac{4Re^{i\pi(1-m)}}{\left(\zeta^2+1\right)^2}(1+\cos\alpha)\left(\zeta - tan\frac{\alpha}{2}\right)^m \left(\zeta + tan\frac{\alpha}{2}\right)^{-m} \times \left\{\zeta + \left[tan\frac{\alpha}{2}\left(m + m\zeta^2 + \zeta\ tan\frac{\alpha}{2}\right)\right]\right\}, \quad (4)$$

$$z'' = \omega''\ \zeta\ = 2m\zeta\ \zeta^4 - 1\ tan\frac{\alpha}{2} - \frac{1}{\zeta^2+1^3}\left\{-4m\zeta\ \zeta^2+1\left(tan\frac{\alpha}{2}\right)^3 + 1-3\zeta^2\ \left(tan\frac{\alpha}{2}\right)^4 - \left(tan\frac{\alpha}{2}\right)^2 \times \right.$$

$$\left. \times\left[4\zeta^2 - 3\zeta^4 - 1 + 2m\ \zeta^2+1^{\ 2}\right] + 4R\zeta^2 e^{i\pi\ 1-m}\ \ 3\zeta^2 - 1\ \ 1+\cos\alpha\ \left(\zeta - tan\frac{\alpha}{2}\right)^{m-1}\left(\zeta + tan\frac{\alpha}{2}\right)^{-m-1}\right\}. \quad (5)$$

Assuming the crack surface is free, the boundary conditions of the crack surface can be expressed as:

$$\sigma_{yy}\ t\ - i\sigma_{xy}\ t\ = 0,\ t \in \text{Crack surface}\ , \quad (6)$$

Referring to the work of He [30-31], the corresponding complex function formulas $\varphi_D(\zeta)$ and $\psi_D(\zeta)$ to calculate the stress fields σ_{xx}^D, σ_{yy}^D and σ_{xy}^D generated by a wedge disclination near a bifurcated crack are obtained as:

$$\varphi_D(\zeta) = \frac{D\omega}{2}\left[\omega'(\zeta_i)(\zeta-\zeta_i)ln(\zeta-\zeta_i) - \omega(\zeta)ln\left(\zeta-\overline{\zeta_i}\right) + z_i\ ln\left(\zeta-\overline{\zeta_i}\right)\right], \quad (7)$$

$$\psi_D(\zeta) = \frac{D\omega}{2}\left[-\overline{\omega'(\zeta_i)}\left(\zeta-\overline{\zeta_i}\right)ln\left(\zeta-\overline{\zeta_i}\right) - \overline{z_i}\ ln(\zeta-\zeta_i)\right] + \frac{\overline{\omega}(\zeta)}{\omega'(\zeta)}\frac{D\omega}{2}\left[\omega'(\zeta)ln\left(\zeta-\overline{\zeta_i}\right) + \frac{\omega(\zeta)}{\zeta-\overline{\zeta_i}} - \frac{z_i}{\zeta-\overline{\zeta_i}}\right], \quad (8)$$

where: $D = \mu/\left[2\pi(1-\nu)\right]$ and $z_i = \omega(\zeta_i)$.

Upon taking the derivative, the following result is obtained as:

$$\varphi_D{}'(\zeta) = \frac{D\omega}{2}\left[\omega'(\zeta_i)ln(\zeta-\zeta_i) + \omega'(\zeta_i) - \omega'(\zeta)ln\left(\zeta-\overline{\zeta_i}\right) - \frac{\omega(\zeta)}{\zeta-\overline{\zeta_i}} + \frac{z_i}{\zeta-\overline{\zeta_i}}\right], \quad (9)$$

$$\varphi_D{}''(\zeta) = \frac{D\omega}{2}\left[\frac{\omega'(\zeta_i)}{\zeta-\zeta_i} - \frac{\omega'(\zeta)}{\zeta-\overline{\zeta_i}} - \omega''(\zeta)ln\left(\zeta-\overline{\zeta_i}\right) + \frac{\omega(\zeta)}{\left(\zeta-\overline{\zeta_i}\right)^2} - \frac{z_i}{\left(\zeta-\overline{\zeta_i}\right)^2}\right], \quad (10)$$

$$\psi_D'(\zeta)=\frac{\overline{\omega}'(\zeta)\omega'(\zeta))-\overline{\omega}(\zeta)\omega''(\zeta)}{\left[\omega'(\zeta)\right]^2}\times\frac{D\omega}{2}\left[\omega'(\zeta)ln\left(\zeta-\overline{\zeta_i}\right)+\frac{\omega(\zeta)}{\zeta-\overline{\zeta_i}}-\frac{z_i}{\zeta-\overline{\zeta_i}}\right]+\frac{\overline{\omega}(\zeta)}{\omega'(\zeta)}\frac{D\omega}{2}\times$$

$$\times\left[\omega''(\zeta)ln\left(\zeta-\overline{\zeta_i}\right)+\frac{2\omega'(\zeta)}{\zeta-\overline{\zeta_i}}-\frac{\omega(\zeta)}{\left(\zeta-\overline{\zeta_i}\right)^2}+\frac{z_i}{\left(\zeta-\overline{\zeta_i}\right)^2}\right]+\frac{D\omega}{2}\left[-\overline{\omega'(\zeta_i)}ln\left(\zeta-\overline{\zeta_i}\right)-\overline{\omega'(\zeta_i)}-\frac{z_i}{\zeta-\zeta_i}\right]. \quad (11)$$

So, the stress field σ_{xx}^N, σ_{yy}^N and σ_{xy}^N caused by nanoscale amorphization near the bifurcated crack can be calculated, see Eqs. (11)-(13). By substituting the stress field obtained above into Eq. (1), the force generated by nanoscale amorphization can be determined.

$$\sigma_{xx}^N(x,y)=\frac{1}{s}\int_0^s\left(\sigma_{x'x'}^D(x',y',x_i',y_i')\big|_{y_i'=0}-\sigma_{x'x'}^D(x',y',x_i',y_i')\big|_{y_i'=d}\right)dx', \quad (12)$$

$$\sigma_{yy}^N(x,y)=\frac{1}{s}\int_0^s\left(\sigma_{y'y'}^D(x',y',x_i',y_i')\big|_{y_i'=0}-\sigma_{y'y'}^D(x',y',x_i',y_i')\big|_{y_i'=d}\right)dx', \quad (13)$$

$$\sigma_{xy}^N(x,y)=\frac{1}{s}\int_0^s\left(\sigma_{x'y'}^D(x',y',x_i',y_i')\big|_{y_i'=0}-\sigma_{x'y'}^D(x',y',x_i',y_i')\big|_{y_i'=d}\right)dx', \quad (14)$$

where: $z=x+iy=x_A+iy_A+\left(x'+iy'\right)e^{i(\alpha-\pi/2)}$.

Secondly, the force generated by the dislocation itself is calculated. The elastic stress field produced by an edge dislocation emitted from a bifurcation crack tip can be represented using complex potentials $\varphi_E(\zeta)$ and $\psi_E(\zeta)$ as [32-34]:

$$\varphi_E(\zeta)=\gamma ln(\zeta-\zeta_0)-\frac{\overline{\gamma}\overline{W}}{\zeta-\overline{\zeta_0}}-\gamma ln\left(-\zeta-\overline{\zeta_0}\right), \quad (15)$$

$$\psi_E(\zeta)=\frac{\overline{\omega}(\zeta)}{\omega'(\zeta)}\left[\frac{\gamma}{\zeta-\overline{\zeta_0}}-\frac{\overline{\gamma}\overline{W}}{\left(-\zeta-\overline{\zeta_0}\right)^2}\right]-$$
$$-\frac{\gamma H}{\zeta-\zeta_0}+\overline{\gamma}ln(\zeta-\zeta_0)-\overline{\gamma}ln\left(\zeta-\overline{\zeta_0}\right). \quad (16)$$

where: $\gamma=\mu\left(b_y-ib_x\right)/\left[4\pi(1-\nu)\right]$, $H=\overline{\omega(\zeta_0)}/\omega'(\zeta_0)$, $W=\left[\overline{\omega}(\zeta_0)-\overline{\omega(\zeta_0)}\right]/\omega'(\zeta_0)$.

Then, the image force f_{Ie} of the dislocation itself can be calculated by Peach-Koehler formula as [35-38]:

$$f_{IE}=f_{IEx}-if_{IEy}=\left[\hat{\sigma}_{xy}(\zeta_0)b_x+\hat{\sigma}_{yy}(\zeta_0)b_y\right]+i\left[\hat{\sigma}_{xx}(\zeta_0)b_x+\hat{\sigma}_{xy}(\zeta_0)b_y\right]=$$
$$=\frac{\mu b^2}{4\pi(1-\upsilon_1)}\left[\frac{\Phi_E^*(\zeta_0)+\overline{\Phi_E^*(\zeta_0)}}{\gamma}+\frac{\overline{\omega(\zeta_0)}\Phi_E^{*\prime}(\zeta_0)+\Psi_E^*(\zeta_0)}{\overline{\gamma}}\right], \quad (17)$$

where: $\hat{\sigma}_{xx}$, $\hat{\sigma}_{xy}$ and $\hat{\sigma}_{yy}$ – the components of disturbance stress generated by the interaction between edge dislocations and bifurcated cracks and

$$\left.\begin{aligned}\Phi_E^*(\zeta_0)&=\frac{\varphi_E'(\zeta_0)}{\omega'(\zeta_0)}\\ \Psi_E^*(\zeta_0)&=\frac{\psi_E'(\zeta_0)}{\omega'(\zeta_0)}\\ \Phi_E^{*\prime}(\zeta_0)&=\frac{\varphi_E''(\zeta_0)\omega'(\zeta_0)-\varphi_E'(\zeta_0)\omega''(\zeta_0)}{\left[\omega'(\zeta_0)\right]^3}\end{aligned}\right\}. \quad (18)$$

Finally, the calculation formula for the force acting on the first edge dislocation, which is induced by in-plane tensile loads (Mode I) and shear loads (Mode II) that are applied at an infinite distance, can be expressed as follows [38, 41]:

$$f_{\Gamma E}=b\sigma_{r\theta}^{\Gamma}=\frac{b}{\sqrt{2\pi r_0}}\left(l_1K_{\mathrm{I}}^N+l_2K_{\mathrm{II}}^N\right), \quad (19)$$

where: $l_1=\frac{1}{2}sin\theta_0\,cos\frac{\theta_0}{2}$, $l_2=cos\frac{3\theta_0}{2}+sin^2\frac{\theta_0}{2}cos\frac{\theta_0}{2}$, K_{I}^N and K_{II}^N are the Mode I and Mode II SIFs at the crack tip under infinite load.

Combining Eqs. (1), (16) and (17), the resultant force acting on the edge dislocation emitted from the tip of the bifurcated crack can be calculated as:

$$f_E=f_{AE}+f_{IE}+f_{\Gamma E}=$$
$$=Re\left[f_{AE}+f_{IE}\right]cos\theta-$$
$$-Im\left[f_{AE}+f_{IE}\right]sin\theta+f_{\Gamma}. \quad (20)$$

4. Analysis of Critical SIF Corresponding to Dislocation Emission

According to the criterion for dislocation emission at the crack tip, the critical condition is met when the force acting on the dislocation is zero, and the distance between the crack and the dislocation must be greater than or equal to the dislocation core radius. By combining the formula for the image force, the forces generated by nanoscale amorphization, and those by external loads, the critical conditions for dislocation emission $f_E = 0$, the expression for the critical SIF corresponding to the dislocation emission from a bifurcation crack tip can be obtained as [25, 30]:

$$K_{\mathrm{II}}^{N} = 0, K_{\mathrm{IC}}^{N} = \frac{\sqrt{2\pi r_0}}{bl_1}\left(Im\left[f_{IE} + f_{AE} \right] sin\theta - Re\left[f_{IE} + f_{AE} \right] cos\theta \right), \tag{21}$$

$$K_{\mathrm{I}}^{N} = 0, K_{\mathrm{IIC}}^{N} = \frac{\sqrt{2\pi r_0}}{bl_2}\left(Im\left[f_{IE} + f_{AE} \right] sin\theta - Re\left[f_{IE} + f_{AE} \right] cos\theta \right). \tag{22}$$

Utilizing the aforementioned formula for the critical SIF associated with dislocation emission, the impact of nanoscale amorphization, crack size, and varying grain sizes on dislocation emission at the tip of the bifurcated crack in nanocrystalline materials can be examined. To streamline the analysis, the critical SIF is rendered dimensionless as $K_{\mathrm{IC}}^{0} = K_{\mathrm{IC}}^{N} / \mu_1 \sqrt{b_r}$ and $K_{\mathrm{IIC}}^{0} = K_{\mathrm{IIC}}^{N} / \mu_1 \sqrt{b_r}$. The size of the nanoscale amorphous region is established as s and d, as well as $s = d$. The classic 3C SiC is chosen as the nanocrystalline material, featuring a shear modulus of $\mu = 217$ GPa and a Poisson's ratio of $\nu = 0.23$.

The strength of the wedge disclination is set as $\pm\omega$, the Burgers vector of the dislocation is assigned as $b = 0.25$ nm [33], and the distance between the bifurcation crack tip and the emitted dislocation is defined as $r_0 = b/2$. When $m = 0$, the main crack and branched crack extend into a straight crack, which is consistent with the research results obtained by Fang [33].

The variation curve of dimensionless critical SIF with dislocation strength is depicted in Fig. 2 when $\alpha = 30°$, $r_1 = 0.15$ nm, $\theta_1 = 0°$, $\theta_0 = 30°$, $b/a = 0.3$, $m = 1/3$, $s = d = 15$ nm. As shown in the figure, with the increase of dislocation strength, both the Mode I and Mode II dimensionless critical SIFs both increases. This indicates that the presence of nanoscale amorphization can reduce the high stress field near the bifurcated crack tip, making it difficult for dislocations to emit from the bifurcated crack tip, thereby reducing the toughness of the material caused by dislocation emission. When the dislocation strength is constant, the Mode I dimensionless SIF is greater than the Mode II dimensionless critical SIF, indicating that shear load is more likely to release dislocations from the tip of the bifurcated crack than tensile load.

The variation curve of the dimensionless critical SIFs with dislocation emission angle at different relative crack lengths b/a is depicted in Fig. 3 when $\alpha = 30°$, $r_1 = 0.15$ nm, $\theta_1 = 0°$, $\omega = 5°$, $m = 1/3$, $s = d = 15$ nm. From Fig. 3, a, the Mode I dimensionless critical SIF increases from infinity to a minimum value, and then increases in the opposite direction to infinity with the increase of dislocation emission angle. The minimum value of K_{IC}^{0} corresponds to the most probable emission angle of dislocations θ_e, which can be obtained from the figure that $\theta_e = 57.5°$at this point, and this critical dislocation emission angle is independent of the relative length of the crack. As the relative crack length b/a increases, it will become increasingly difficult for dislocations to emit from the bifurcation crack tip.

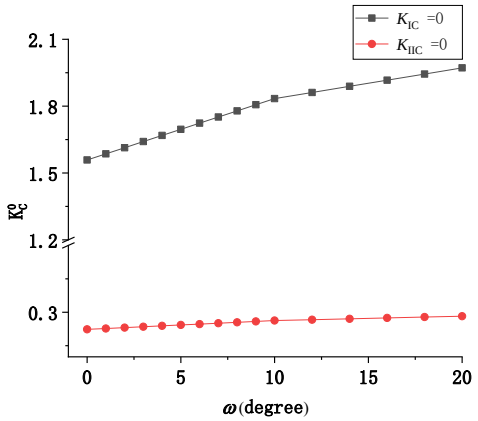

Fig. 2 Dependence of the dimensionless critical SIFs K_C^0 with dislocation strength ω

From Fig. 3, b, it can be seen that the Model II critical SIF first increases from a finite positive value to infinity and then transitions to a negative value as the emission angle increases. The sign of the critical SIF is determined by the direction of Burgers vector of the emitting dislocation [35]. So, for positive edge dislocations, the most probable emission angle is zero. The negative critical SIF initially decreases to a minimum value and subsequently increases as the dislocation emission angle increases. The most probable angle for negative dislocations to emanate from the bifurcated crack tip is also at $\theta = 57.5°$. As the relative crack length increases, it becomes more challenging for dislocations to emit from the bifurcated crack tip.

The variation curve of the dimensionless critical SIF with dislocation emission angle at different m is depicted in Fig. 4 when $\alpha = 30°$, $r_1 = 0.15$ nm, $b/a = 0.3$, $\theta_1 = 0°$, $\omega = 5°$, $s = d = 15$ nm. From Fig. 4, a, the Mode I critical SIF increases from infinity to a minimum value and then increases in the opposite direction to infinity as the dislocation emission angle increases. The most probable emission angle corresponding to the minimum value is $\theta_e = 58.5°$, independent of the value of m. As the value of m increases, it becomes increasingly challenging for dislocations to emit from the tip of the bifurcated crack. From Fig. 4, b, it is evident that the critical SIF for Mode II decreases from a finite positive value to a negative value as the emission angle of the edge dislocation increases, and subsequently rises from a negative value to a positive infinite value. The most probable angle for dislocation emission

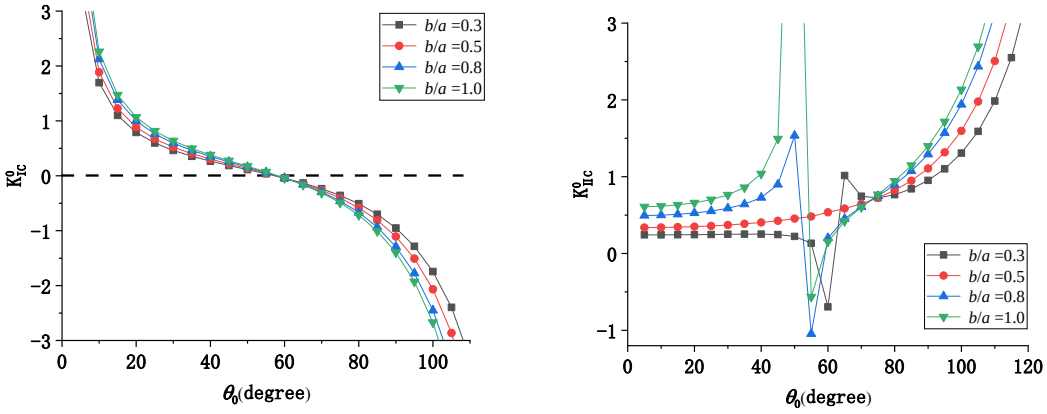

a b

Fig. 3 Dependence of the dimensionless critical SIFs on the edge dislocation emission angle θ_0 with different relative crack lengths b/a: a – K^0_{IC}, b – K^0_{IIC}

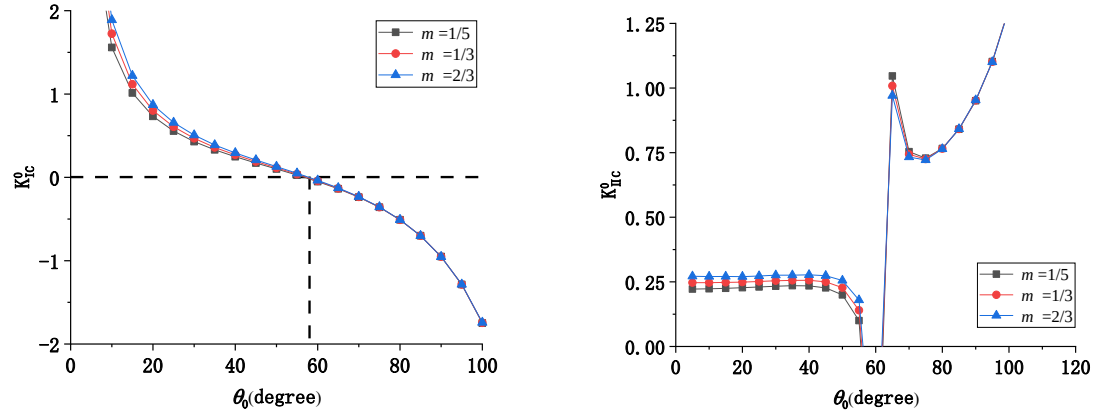

a b

Fig. 4 Dependence of the dimensionless critical SIFs on the edge dislocation emission angle θ_0 with different m: a – K^0_{IC}, b – K^0_{IIC}

from the bifurcated crack tip is at θ_e = 57°and θ_e = 62.5°. As the value of m increases, the dimensionless critical SIF also increases. This suggests that as the angle between the main crack and the branched crack increases, dislocation emission from the branched crack tip becomes more difficult.

As shown in Fig. 5, the variation curve of the dimensionless critical SIF with the nanoscale amorphous size d is depicted when different dislocation strengths are taken, and α = 30°, r_1 = 0.15 nm, b/a = 0.3, θ_1 = 0°, ω = 5°, m = 1/3, s = 15 nm. As shown in the figure, with the increase of nanoscale amorphous size, the critical SIF increases under the action of Mode I load and eventually tends to remain constant. When there is no nanoscale amorphous deformation at the crack tip (ω = 0°), the critical SIF remains a constant. And when the nanoscale amorphous size is small, the critical SIF of dislocation emission is greatly affected, which makes it difficult to emit dislocations at the tip of the bifurcated crack. However, when the size is large, the increase in grain size has little effect on the critical SIF.

As depicted in Fig. 6, the variation curve of the dimensionless critical SIF with the nanoscale amorphization size d is illustrated for different nanoscale amorphization azimuth angles when r_1 = 0.15 nm, b/a = 0.3, θ_1 = 0°, ω = 5°, m = 1/3, s = 15 nm. The figure reveals that as the azimuth angle of nanoscale amorphization increases, the critical SIF initially decreases and subsequently increases, indicating a minimum nanoscale amorphization size d_0 corresponding to

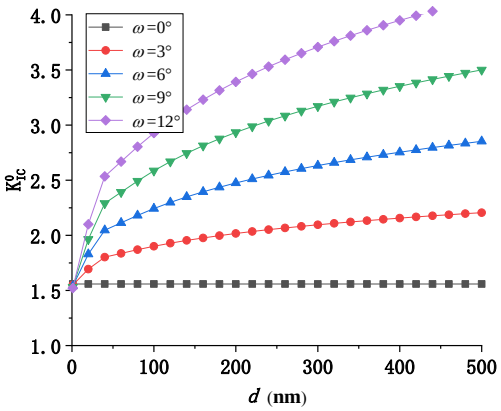

Fig. 5 Dependence of the normalized critical SIF K^0_{IC} on the nanoscale amorphization size with different disclination strength ω

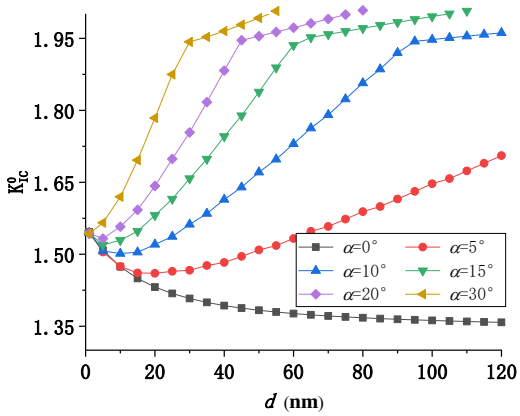

Fig. 6 Dependence of the dimensionless critical SIF K_{IC}^0 on the nanoscale amorphization size with different nanoscale amorphization azimuth angle α

the lowest critical SIF. When the inclination angle of nanoscale amorphization is $\alpha = 5°$, the corresponding minimum nanoscale amorphization size is d_0 =17; for $\alpha = 10°$, d_0 =11; for $\alpha = 15°$, d_0 =4; and for $\alpha = 20°$, d_0 =2. It is evident that increasing the nanoscale amorphization size can reduce the corresponding critical SIF. Consequently, nanoscale amorphization facilitates the emission of dislocations at the tips of branched cracks, thereby enhancing the fracture toughness of materials.

5. Conclusions

The present study has provided a comprehensive analysis of the influence of nanoscale amorphization on the dislocation emission behavior at the tips of bifurcated cracks. The force acting on the dislocation was derived using the complex potential method of elastic mechanics, including the image force of the dislocation itself, the force generated by amorphization, and the force generated by external loading. Based on the dislocation emission conditions, an analytical expression for the critical SIF corresponding to dislocation emission was obtained, and the effects of relative crack length, angle between the main crack and the branched crack, strength of nanoscale amorphization, and dislocation emission angle on the critical Mode I and Mode II SIFs were discussed. The conclusion is summarized as follows:

1. The presence of nanoscale amorphization reduces the high stress field near the bifurcated crack tip, suppressing dislocation emission from the crack tip. This suppression of dislocation activity diminishes the material's ability to undergo plastic deformation, thereby reducing its toughness.

2. As the relative crack length b/a increases, it becomes increasingly difficult for dislocations to emit from the bifurcated crack tip. This trend suggests that longer branched cracks can act as more effective barriers to dislocation motion, potentially enhancing the material's strength but at the expense of ductility.

3. A larger angle between the main crack and the bifurcation crack further inhibits dislocation emission from the branched crack tip. This geometric effect implies that crack branching at higher angles can significantly impede plastic deformation, leading to increased brittleness. However, the critical dislocation emission angle remains unaffected by the angle between the main and branched cracks, suggesting that the local stress field near the crack tip governs dislocation nucleation regardless of the global crack geometry.

Acknowledgments

The authors deeply appreciate the support from the National Natural Science Foundation of China (32371807, 11602308) and the key scientific research projects of Hunan Provincial Education Department (20A522, 21A0601).

References

1. **Zhang, Z.; Ódor, É.; Farkas, D.; Jóni, B.; Ribárik, G.; Tichy, G.; Nandam, S. H.; Ivanisenko, J.; Preuss, M.; Ungár, T.** 2020. Dislocations in Grain Boundary Regions: The Origin of Heterogeneous Microstrains in Nanocrystalline Materials, Metallurgical And Materials Transactions A 51: 513-530. https://doi.org/10.1007/s11661-019-05492-7.
2. **Moskalenko, V. A.; Smolianets, R. V.; Natsik, V. D.; Pohribna, Y. M.** 2023. Dislocation mechanisms of low-temperature plasticity of nanocrystalline titanium: The role of impurity and grain boundary strengthening, Low Temperature Physics 49(2): 248. https://doi.org/10.1063/10.0016852.
3. **Cappola, J.; Wang, J.; Li, L**. 2024. A dislocation-density-based crystal plasticity model for FCC nanocrystalline metals incorporating thermally-activated depinning from grain boundaries, International Journal of Plasticity 172: 103863. https://doi.org/10.1016/j.ijplas.2023.103863.
4. **Yang, Z.; Yang, F.** 2023. Scattering of phonons by edge dislocation and thermal conductivity of nanocrystalline silicon, Micro and Nanostructures 180: 207608. https://doi.org/10.1016/j.micrna.2023.207608.
5. **Lu, X.; Zhang, W.; Ren, J.; Gao, Q.; Xue, H.; Tang, F.; La, P.; Guo, X.** 2023. Grain boundary segregation strengthening behavior caused by carbon chain network formation in nanocrystalline NiCoAl alloy, Journal of Materials Research and Technology 26: 1016-1027. https://doi.org/10.1016/j.jmrt.2023.07.232.
6. **Gan, K.; Yan, D.; Zhang, Y.; Li, Z.** 2023. Origins of strengthening and toughening effects in twinned nanocrystalline alloys of low stacking fault energy with heterogeneous grain structure, Journal of the Mechanics and Physics of Solids 176: 105305. https://doi.org/10.1016/j.jmps.2023.105305.
7. **Cai, J.; Griesbach, C.; Ahnen, S. G.; Thevamaran, R.** 2023. Dynamic Hardness Evolution in Metals from Impact Induced Gradient Dislocation Density, Acta Materialia 249: 118807. https://doi.org/10.1016/j.actamat.2023.118807.
8. **Hasan, M. S.; Lee, R.; Xu, W.** 2020. Deformation nanomechanics and dislocation quantification at the atomic scale in nanocrystalline magnesium, Journal of Magnesium and Alloys 8(4): 1296-1303. https://doi.org/10.1016/j.jma.2020.08.014.
9. **Gubicza, J.** 2020. Annealing-Induced Hardening in Ultrafine-Grained and Nanocrystalline Materials, Advanced Engineering Materials 22(1): 1900507.

https://doi.org/10.1002/adem.201900507.
10. **Wolf, D.; Yamakov, V.; Phillpot, S.R.; Mukherjee, A. K.** 2022. Deformation mechanism and inverse Hall–Petch behavior in nanocrystalline materials, International Journal of Materials Research 94(10): 1091-1097. https://doi.org/10.1515/ijmr-2003-0199.
11. **Li, J. C. M.; Feng, C. R.; Rath, B. B.** 2020. Emission of Dislocations from Grain Boundaries and Its Role in Nanomaterials, Crystals 11(1): 41. https://doi.org/10.3390/cryst11010041.
12. **Naik, S. N.; Walley, S. M.** 2020. The Hall-Petch and inverse Hall-Petch relations and the hardness of nanocrystalline metals, Journal of Materials Science 55(7): 2661-2681. https://doi.org/10.1007/s10853-019-04160-w.
13. **Sun, S.; Yang, Y.; Han, C.; Sun, G.; Chen, Y.; Zong, H.; Hu, J.; Han, S.; Liao, X.; Ding, X.; Lian, J.** 2022. Unveiling the grain boundary-related effects on the incipient plasticity and dislocation behavior in nanocrystalline CrCoNi medium-entropy alloy, Journal of Materials Science & Technology 127: 98-107. https://doi.org/10.1016/j.jmst.2022.02.041.
14. **Lin, H.; Hua, P.; Huang, K.; Li, Q.; Sun, Q.** 2023. Grain boundary and dislocation strengthening of nanocrystalline NiTi for stable elastocaloric cooling, Scripta Materialia 226: 115227. https://doi.org/10.1016/j.scriptamat.2022.115227.
15. **Karafi, T.; Tahiri, A.; Chabba, H.; Idiri, M.; Boubeker, B.** 2023. Effect of Grain-Size in Nanocrystalline Tungsten on Hardness and Dislocation Density: A Molecular Dynamics Study, Crystals 13(3): 469. https://doi.org/10.3390/cryst13030469.
16. **Renk, O.; Hohenwarter, A.; Maier-Kiener, V.; Pippan, R.** 2023. Exploring the anneal hardening phenomenon in nanocrystalline Pt-Ru alloys, Journal of Alloys and Compounds 935: 168005. https://doi.org/10.1016/j.jallcom.2022.168005.
17. **Yao, H.; Ye, T.; Wang, P.; Wu, J.; Zhang, J.; Chen, P.** 2023. Structural Evolution and Transitions of Mechanisms in Creep Deformation of Nanocrystalline FeCrAl Alloys, Nanomaterials 13(4): 631. https://doi.org/10.3390/nano13040631.
18. **Chen, Y.; Liu, M.; Ding, L.; Jia, Z.; Jia, S.; Wang, J.; Murashkin, M.; Valiev, R. Z.; Roven, H. J.** 2023. Atomic-scale inhomogeneous solute distribution in an ultrahigh strength nanocrystalline Al-8 Mg aluminum alloy, Materials Characterization 198: 112706. https://doi.org/10.1016/j.matchar.2023.112706.
19. **Allahverdi, E.; Soleimanian, V.; Ghasemi, M.; Mokhtari, A.** 2023. Microstructure and optical properties of NaTaO3 and TiO2 nanocrystalline low symmetry materials, Materials Science in Semiconductor Processing 153: 107106. https://doi.org/10.1016/j.mssp.2022.107106.
20. **Jiang, J.; Sun, W.; Luo, N.; Chen, P.** 2023. Atomic-scale analysis of deformation behavior of face-centered cubic nanocrystalline high-entropy alloys with different grain sizes at high strain rates, Materials Chemistry and Physics 300: 127556. https://doi.org/10.1016/j.matchemphys.2023.127556.
21. **Hu, K.; Yi, J.; Huang, B.; Wang, G.** 2023. Grain-size effect on dislocation source-limited hardening and ductilization in bulk pure Ni, Journal of Materials Science & Technology 154: 9-21. https://doi.org/10.1016/j.jmst.2022.12.044.
22. **Zhang, W.; Lu, X.; Ren, J.; Li, J.; Xue, H.; Tang, F.; Guo, X.** 2023. Effect of Al Segregation on Mechanical Properties and Deformation Mechanism of Nanocrystalline NiCoAl, Crystal Growth & Design 23(6): 4621-4628. https://doi.org/10.1021/acs.cgd.3c00374.
23. **Feng, H.; Fang, Q. H.; Liu, Y. W.; Chen, C. P.** 2014. Nanoscale rotational deformation effect on dislocation emission from an elliptically blunted crack tip in nanocrystalline materials, International Journal of Solids and Structures 51: 352-358. https://doi.org/10.1016/j.ijsolstr.2013.10.008.
24. **Feng, H.; Fang, Q. H.; Liu, B.; Liu, Y.; Liu, Y. W.; Wen, P. H.** 2017. Nucleation and growth mechanisms of nanoscale deformation twins in hexagonal-close-packed metal magnesium, Mechanics of Materials 109: 26-33. https://doi.org/10.1016/j.mechmat.2017.03.015.
25. **Feng, H.; Tang, J.; Peng, J.; Wu, H.** 2019. Nanoscale amorphization effect on dislocation emission from an elliptical blunt crack tip in deformed nanocrystalline and ultrafine-grained materials, Mechanics of Materials 134(7): 98-105. https://doi.org/10.1016/j.mechmat.2019.04.019.
26. **Ovid'ko, I. A.; Sheinerman, A. G.** 2010. Ductile vs. brittle behavior of pre-cracked nanocrystalline and ultrafine-grained materials, Acta Materialia 58(16): 5286-5294. https://doi.org/10.1016/j.actamat.2010.05.058.
27. **Ovid'ko, I. A.; Sheinerman, A. G.** 2016. Free surface effects on stress-driven grain boundary sliding and migration processes in nanocrystalline materials, Acta Materialia 121: 117-125. https://doi.org/10.1016/j.actamat.2016.08.082.
28. **Ovid'ko, I. A.; Sheinerman, A. G.** 2012. Nanoscale amorphization near crack tips in deformed nanocrystalline and ultrafine grained solids, Reviews on Advanced Materials Science 32: 61-67.
29. **Ovid'ko, I. A.** 2012. Nanoscale amorphization as a special deformation mode in nanowires, Scripta Materialia 66(6): 402-405. https://doi.org/10.1016/j.scriptamat.2011.12.001.
30. **He, T. W.; Xiao, W. S.; Zhang, Y.; Zhu, H. P.** 2017. Effect of special rotational deformation on the dislocation emission from a branched crack tip in deformed nanocrystalline materials, Acta Mechanica 228: 823-836. https://doi.org/10.1007/s00707-016-1742-y.
31. **He, T. W.; Feng, M. L.** 2018. Effect of nanotwin near a branched crack tip on crack blunting in deformed nanocrystalline materials, Acta Mechanica 229: 3223-3234. https://doi.org/10.1007/s00707-018-2158-7.
32. **Kuntz, J. D.; Zhan, G. D.; Mukherjee, A. K.** 2004. Nanocrystalline-Matrix Ceramic Composites for Improved Fracture Toughness, MRS Bulletin 29: 22-27. https://doi.org/10.1557/mrs2004.12.
33. **Fang, Q. H.; Liu, Y. W.; Jiang, C. P.; Li, B.** 2006. Interaction of a wedge disclination dipole with interfacial cracks, Engineering Fracture Mechanics 73(9): 1235-1248. https://doi.org/10.1016/j.engfracmech.2005.12.010.
34. **Yang, F.; Yang, W.** 2009. Crack growth versus blunting in nanocrystalline metals with extremely small grain size, Journal of the Mechanics and Physics of Solids 57(2):

305-324.
https://doi.org/10.1016/j.jmps.2008.10.011.
35. **Zhang, T. Y.; Li, J. C. M.** 1992. Interaction of an edge dislocation with an interfacial crack, Journal of Applied Physics 72(6): 2215-2227.
https://doi.org/10.1063/1.351614.
36. **Rice, J. R.; Thomson, R.** 1974. Ductile versus brittle behavior of crystals, The Philosophical Magazine: A Journal of Theoretical Experimental and Applied Physics 29(1): 73-97.
https://doi.org/10.1080/14786437408213555.
37. **Sih, G. C.** 1965. Stress Distribution Near Internal Crack Tips for Longitudinal Shear Problems, ASME Journal of Applied Mechanics 32(1): 51-58.
https://doi.org/10.1115/1.3625783.
38. **Hirth, J. P.; Lothe, J.; Mura, T.** 1983. Theory of dislocations (2nd ed.), ASME Journal of Applied Mechanics 50(2): 476-477.
https://doi.org/10.1115/1.3167075.

X. Song, M. Yu, X. Peng

EFFECT OF NANOSCALE AMORPHIZATION ON EDGE DISLOCATION EMISSION FROM A BIFURCATED CRACK TIP IN DEFORMED NANOCRYSTALLINE SOLIDS

S u m m a r y

The effect of nanoscale amorphization at the triple junction of grain boundaries on edge dislocation emission from a bifurcated crack tip in nanocrystalline materials has been suggested and theoretically described. A corresponding mechanical model has been established, and the exact analytical solution of the modified model was obtained using the complex potential method of elastic mechanics. The resultant force acting on the dislocation was calculated, and the analytical expression for the critical SIF corresponding to dislocation emission was obtained based on the dislocation emission criterion. The influence of the size, position, strength of nanoscale amorphization, and bifurcated crack shape on the critical SIF was discussed using numerical analysis. The study found that an increase in the angle between the main crack and the branched crack makes it more difficult for dislocations to emit from the bifurcated crack tip. The critical dislocation emission angle is independent of the angle between the main crack and the branched crack. The presence of nanoscale amorphization can reduce the high stress field near the bifurcated crack tip, making it difficult for dislocations to emit from the bifurcated crack tip, thereby reducing the toughness of the material caused by dislocation emission.

Keywords: nanoscale amorphization, bifurcated crack, dislocation emission, stress intensity factor, complex potential solution method, nanocrystalline solid.

Received January 16, 2025
Accepted April 22, 2025